IJSES
International Journal of Scientific Engineering and Science
Volume 10, Issue 9, pp. 32-40, September 2026.
ISSN (Online): 2456-7361

Dual-Function 2×2 MIMO Patch Antenna for Combinning V2X Communication and Automotive Radar Applications

Mohammad Shahed Pervez[1] *, Kamran Mohammed[2], Amanpreet Kaur, Ph.D[3]
[1]Department of Electrical and Computer Engineering, Oakland University, Rochester, Michigan, USA
[2]North America Battery Management System, Stellantis (FCA US LLC), Auburn Hills, USA
[3]Assistant Professor, Department of Electrical and Computer Engineering, Oakland University, Rochester, Michigan, USA

Abstract— *This paper develops the dual-function 2×2 MIMO microstrip patch antenna originally presented as a compact platform for joint vehicle-to-everything (V2X) communication and automotive radar. The architecture combines 5.9 GHz communication and 24 GHz sensing elements within a shared planar aperture on a low-loss Rogers RT5880 substrate. Independent inset-fed rectangular patches are arranged in an interleaved configuration so that the lower-frequency elements support V2X operation while the higher-frequency elements provide a more directive radar aperture. A defected ground structure (DGS) is incorporated between neighboring elements to suppress surface-wave propagation and reduce mutual coupling without increasing the overall footprint. The design is evaluated in Ansys HFSS using a Driven Modal formulation, radiation boundaries, adaptive meshing, and frequency sweeps covering both operating regions. The reported simulations show minimum reflection coefficients of −27 dB at 5.9 GHz and −22 dB at 24 GHz, inter-element isolation better than 18 dB, envelope correlation coefficient (ECC) below 0.05, and peak gains of approximately 7.5 dBi and 14.9 dBi at 5.9 and 24 GHz, respectively. The extended analysis emphasizes the interaction among impedance matching, isolation, diversity, radiation behavior, and vehicular integration, and identifies experimental validation, beamforming, larger arrays, and higher-frequency radar operation as logical next steps.*

Keywords— *V2X communication, automotive radar, MIMO antennas, dual-band antennas, defected ground structure, integrated sensing and communication, 5.9 GHz, 24 GHz.*

I. INTRODUCTION

Connected and autonomous vehicles increasingly require communication and sensing functions to operate concurrently. V2X communication provides a wireless link for exchanging information among vehicles, roadside infrastructure, pedestrians, and other transportation-system entities, while automotive radar supplies local environmental awareness through radio-frequency sensing. In a conventional vehicle architecture, these functions can be implemented with separate antenna modules. Although functionally straightforward, this approach increases the number of RF interfaces, occupied installation area, cabling, and integration constraints. A shared antenna platform is therefore attractive when it can preserve the electromagnetic requirements of both services.

The source identifies 5.9 GHz for V2X communication and 24 GHz for short-range automotive radar. Their very different electrical sizes create a shared-aperture challenge. The proposed solution uses independently tuned interleaved rectangular patches rather than forcing both resonances into one radiator.

MIMO techniques further strengthen the case for a shared aperture. Multiple spatial channels can improve communication reliability and support beamforming, while multiple radar elements can provide additional spatial information and enable more directional radiation. The conference paper identified a gap in physically realizable dual-band MIMO antennas that evaluate both electromagnetic and MIMO-level performance for vehicular use. This journal extension develops that design rationale in greater detail and organizes the reported HFSS results into a unified performance framework.

The principal contributions are: (1) a compact 80 mm × 80 mm dual-function 2×2 planar architecture; (2) interleaved 5.9 GHz and 24 GHz patch elements with independent 50-Ω excitation; (3) DGS-based isolation enhancement between neighboring radiators; (4) simultaneous evaluation of S-parameters, isolation, ECC, radiation patterns, and gain; and (5) an integrated discussion of the design's suitability and remaining limitations for practical vehicular deployment.

II. BACKGROUND AND DESIGN REQUIREMENTS

The antenna must satisfy requirements that are normally considered separately for communications and radar. For the V2X function, the lower-frequency radiator should provide a stable radiation pattern and adequate impedance matching across the intended communication band. For radar, the 24 GHz radiator should provide stronger directivity and useful gain. At the MIMO level, the elements should exhibit low mutual coupling so that the signals associated with different ports remain sufficiently independent. The system-level motivation is consistent with prior IEEE work on vehicular mmWave communication, automotive radar, and joint communication-radar systems [2], [3], [7], [9], [12].

The design therefore follows four coupled requirements. First, the resonant behavior of the 5.9 GHz and 24 GHz elements must remain distinct. Second, the feed structures must provide controlled 50-Ω excitation. Third, the ground plane must be engineered to limit unwanted surface-wave coupling between adjacent elements. Fourth, the resulting

Volume 10, Issue 9, pp. 32-40, September 2026. ISSN (Online): 2456-7361

radiation patterns and diversity metrics must remain suitable for the two different vehicular functions.

Table 1 summarizes the parameters explicitly reported in the source conference manuscript. Detailed individual patch dimensions, DGS slot dimensions, and fabricated-material tolerances are not specified in the source and are therefore not introduced here as measured or simulated facts.

TABLE 1: Design Parameters Summarization

Parameter	Reported design target result
Overall antenna footprint	80 mm × 80 mm
Lower operating band	5.9 GHz (V2X / DSRC)
Higher operating band	24 GHz (automotive radar)
Configuration	2×2 MIMO, interleaved dual-band patches
Substrate	Low-loss Rogers RT5880; source describes $\varepsilon r \approx 2.2$–2.9
Excitation	50-Ω coaxial-fed wave ports
Solver	Ansys HFSS Driven Modal
Frequency coverage	5–30 GHz adaptive sweep
Isolation	Better than 18 dB across both bands
ECC	Below 0.05
Peak gain	7.5 dBi at 5.9 GHz; 14.9 dBi at 24 GHz

III. PROPOSED ANTENNA ARCHITECTURE

The proposed antenna uses a single-layer dielectric platform with an overall footprint of 80 mm × 80 mm. Four radiating elements are arranged as a 2×2 MIMO system. Two elements are tuned for the lower 5.9 GHz band and two are tuned for 24 GHz. The interleaved placement allows both functions to occupy one planar module while preserving independent excitation paths. The resulting architecture is intentionally modular: the lower-frequency elements form the communication portion of the aperture, while the smaller higher-frequency elements provide the radar-oriented portion.

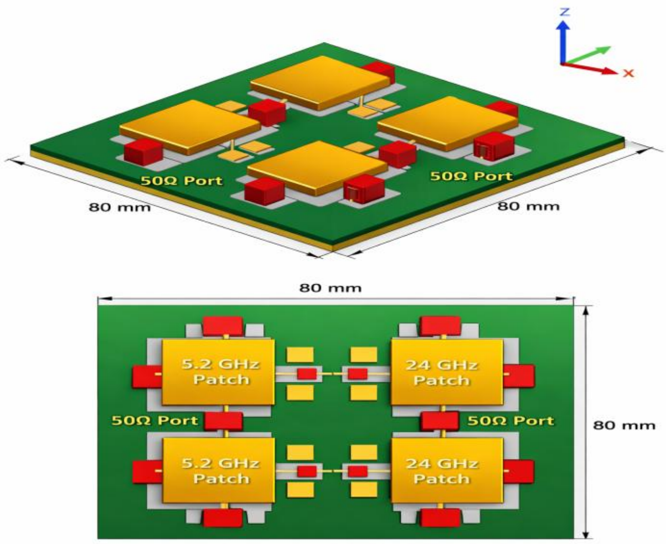

Fig. 1. 3D HFSS model and planar arrangement of the proposed dual-band 2×2 MIMO antenna

Each element is represented in HFSS as a rectangular microstrip patch with an explicit microstrip feed and a coaxial-fed wave port. The 50-Ω wave-port representation provides a controlled reference impedance and allows the full four-port network to be characterized. The feed lines and tuning stubs are retained in the electromagnetic model rather than being represented as ideal lumped matching blocks. This choice is important because the feed geometry participates in the resonance and can also affect coupling between neighboring elements.

A. Interleaved Dual-Band Configuration

The interleaving strategy is central to the compactness of the design. The 5.9 GHz patches occupy the larger electrical footprint expected from their lower operating frequency, while the 24 GHz patches occupy smaller regions within the same overall board. The arrangement avoids a multilayer stacked construction and consequently simplifies the basic physical architecture. The source describes the structure as suitable for vehicular integration because the shared planar aperture reduces the need for separate antenna modules.

An important practical consequence of the interleaving approach is that the lower-frequency and higher-frequency fields can interact through the common ground plane and nearby feed structures even though the resonant elements are individually tuned. The design therefore cannot be evaluated only by S11. Isolation and ECC are essential complementary metrics, and the DGS is introduced specifically to address this interaction.

B. Defected Ground Structure

The DGS consists of etched slots strategically positioned between neighboring elements. Rather than adding bulky external decoupling components, the DGS modifies the electromagnetic behavior of the ground plane. The source describes the slots as producing an effective band-stop behavior that suppresses unwanted surface-wave propagation. This mechanism is especially useful in a closely arranged MIMO structure because surface currents can otherwise provide an unintended coupling path between ports.

The DGS also illustrates the trade-off inherent in MIMO antenna design. Isolation enhancement cannot be considered independently of impedance matching and radiation efficiency. Any modification of the ground current distribution can change the resonant frequency, current confinement, and far-field pattern. The reported design therefore combines DGS geometry with microstrip tuning stubs and parametric optimization rather than treating the isolation structure as a stand-alone addition.

IV. ELECTROMAGNETIC MODELING AND SIMULATION METHODOLOGY

Full-wave three-dimensional simulations were performed in Ansys HFSS using a Driven Modal solver. The computational model includes the dielectric substrate, radiating patches, feed structures, ground plane, DGS features, and surrounding air region. Radiation boundaries are used to emulate free-space radiation. The source specifies an airbox of

International Journal of Scientific Engineering and Science
Volume 10, Issue 9, pp. 32-40, September 2026. ISSN (Online): 2456-7361

approximately λ0/4 at 5.9 GHz and radiation boundaries on all faces.

The reported simulation uses a solution frequency of 6 GHz, with a 5–7 GHz sweep at 0.05 GHz increments and a 22–26 GHz sweep at 0.1 GHz increments. The adaptive mesh criterion is $\Delta S < 0.02$. In addition, the broader methodology describes an adaptive 5–30 GHz sweep to capture both operating regions. These settings provide a common electromagnetic model while allowing the lower- and higher-frequency responses to be resolved with appropriate frequency sampling.

TABLE 2. HFSS Design Conditions

HFSS item	Configuration reported in source
Analysis type	Driven Modal, full-wave 3D
Airbox	Approximately λ0/4 at 5.9 GHz
Boundary	Radiation boundary on all faces
Solution frequency	6 GHz
Lower-band sweep	5–7 GHz, 0.05 GHz step
Radar-band sweep	22–26 GHz, 0.1 GHz step
Adaptive criterion	$\Delta S < 0.02$
Primary outputs	S-parameters, ECC, radiation patterns, gain

The analysis sequence begins with impedance matching and proceeds to coupling and diversity. Reflection coefficients establish whether the individual ports are properly excited. Mutual-coupling terms quantify energy transferred from one element to another. ECC then translates the network behavior into a MIMO diversity indicator. Finally, far-field patterns and gain establish whether the electromagnetic performance is consistent with the intended V2X and radar functions.

A. Parametric Optimization Strategy

The source reports optimization of patch dimensions, feed-line widths, tuning stubs, and DGS geometry. Patch dimensions primarily control resonance, feed dimensions control impedance transformation, and the DGS modifies coupling paths. These variables must therefore be optimized together because a change in one can perturb several metrics.

For a journal-level design workflow, the optimization can be viewed as a sequence of constrained electromagnetic objectives: obtain the desired resonance, maintain acceptable matching, increase inter-element isolation, keep ECC low, and preserve useful radiation characteristics. The conference results indicate that this process produced deeper resonance nulls and wider 10-dB bandwidths at both operating regions when compared with the corresponding stub-less configuration.

V. Results and Discussion

A. Reflection Coefficient and Impedance Matching

Figure 2 presents the simulated S-parameter response. At 5.9 GHz, the minimum reported S11 is approximately −27 dB. At 24 GHz, the corresponding minimum is approximately −22 dB. These values indicate strong impedance matching at both target frequencies and provide substantial margin relative to a −10 dB matching criterion.

The response demonstrates why the feed network is an important part of the antenna rather than a secondary implementation detail. The microstrip tuning stubs compensate for coupling-induced frequency shifts and deepen the resonance nulls. The source further reports wider 10-dB bandwidths at both bands compared with a stub-less configuration. Thus, the feed and radiator must be optimized together to stabilize the dual-band response.

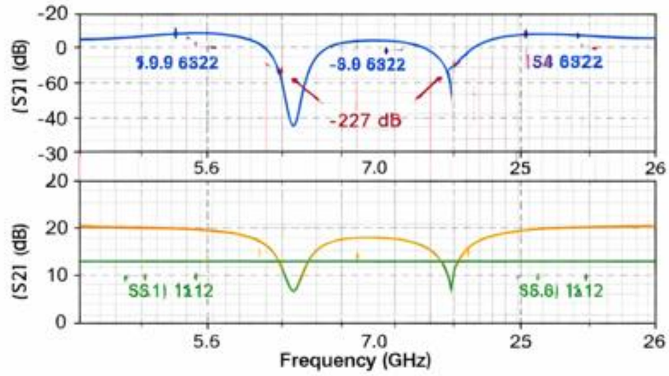

Fig. 2. Simulated S-parameters showing the reported dual-band resonances and inter-element coupling behavior.

The two resonances serve different system functions. The 5.9 GHz response is associated with the V2X communication elements and their relatively broadside radiation behavior. The 24 GHz response is associated with the smaller radar-oriented elements and their more directive radiation. Maintaining separate resonant behavior within one aperture is therefore a central success criterion of the architecture.

B. Mutual Coupling and Isolation

Mutual coupling is particularly important in the proposed structure because four ports share one ground plane. Coupling can distort impedance matching, reduce diversity, and alter the intended radiation patterns. The source reports inter-element isolation exceeding 18 dB across both operating bands. This result is attributed in part to the DGS, which reduces surface-wave propagation between adjacent elements.

The isolation result is significant because it is achieved without increasing the reported 80 mm × 80 mm footprint. Instead, the ground plane itself becomes part of the decoupling network. The approach is consequently compatible with the stated objective of a compact, fabrication-friendly module. Nevertheless, the source does not provide measured S-parameters or a fabrication tolerance study, so the reported isolation should be interpreted as a simulated result rather than a production-qualified value.

C. Envelope Correlation Coefficient

ECC provides a direct indication of the degree to which the radiation responses of MIMO elements are correlated. The source reports ECC below 0.05 across both operating bands. Such a low value indicates that the ports provide highly distinct spatial channels and supports the intended diversity operation.

International Journal of Scientific Engineering and Science
Volume 10, Issue 9, pp. 32-40, September 2026. ISSN (Online): 2456-7361

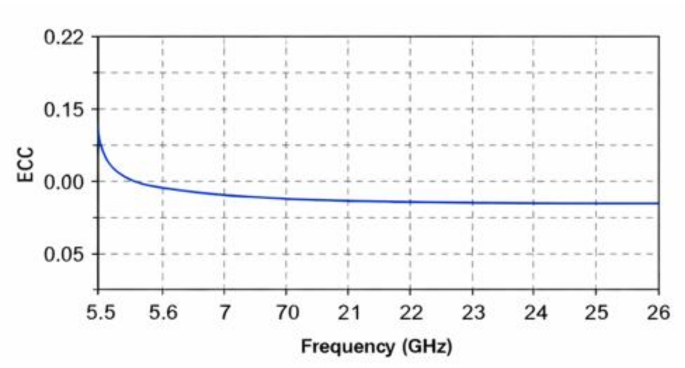

Fig. 3. Simulated envelope correlation coefficient (ECC) reported for the 2×2 MIMO antenna.

The low ECC is consistent with the combined effects of element arrangement, DGS-based coupling suppression, and controlled excitation. Importantly, low ECC should not be interpreted in isolation. A useful MIMO antenna must simultaneously exhibit adequate isolation, acceptable matching, and suitable radiation efficiency. The proposed design meets these criteria in the reported simulation set, which strengthens the case for its use as a shared communication-and-sensing aperture.

D. Radiation Characteristics and Gain

The simulated far-field patterns demonstrate a clear functional distinction between the two operating bands. At 5.9 GHz, the reported pattern is stable and broadly directed toward broadside with low back-lobe radiation. Such behavior is consistent with the communication role, where stable coverage is more important than very narrow directivity. At 24 GHz, the pattern becomes more directive, which is advantageous for radar sensing and for high-data-rate links that can exploit directional transmission.

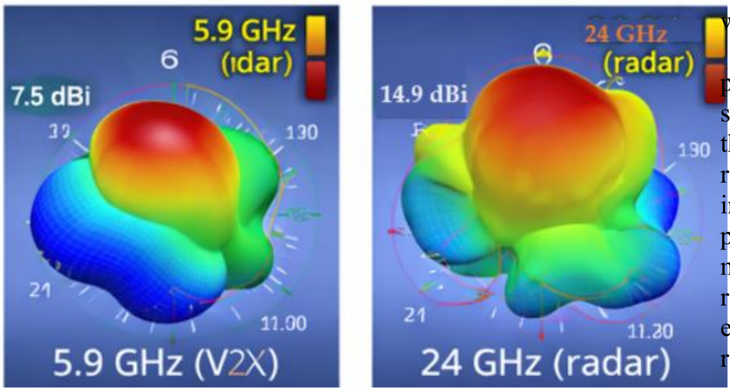

Fig. 4. Simulated three-dimensional radiation patterns and peak gain at 5.9 GHz and 24 GHz.

The reported peak gain is approximately 7.5 dBi at 5.9 GHz and 14.9 dBi at 24 GHz. The substantially higher gain at 24 GHz is attributed in the source to reduced surface-wave losses and improved current confinement on the smaller mmWave radiating elements. This gain separation is also consistent with the different functional requirements: the lower band emphasizes reliable communication coverage, whereas the higher band benefits from a more concentrated sensing aperture.

The radiation results should also be considered together with the isolation results. A decoupling technique that improves S21 but creates severe pattern distortion would not be useful for a joint communication-radar antenna. The reported stable patterns suggest that the DGS and feed optimization provide isolation without undermining the primary radiation characteristics.

TABLE 3. Integrated Performance Assessment

Metric	5.9 GHz	24 GHz	System implication
Resonance	−27 dB S11	−22 dB S11	Strong impedance matching
Isolation	>18 dB	>18 dB	Reduced port-to-port coupling
ECC	<0.05	<0.05	High MIMO diversity potential
Peak gain	7.5 dBi	14.9 dBi	Coverage at V2X / directivity at radar band
Pattern	Broadside, stable	More directive	Different functions supported in shared aperture

Table 3 provides a compact interpretation of the principal reported results. The value of the architecture is not a single record metric but the simultaneous achievement of matching, isolation, low correlation, and useful gain in a single planar antenna. This combination is the basis for describing the antenna as dual-function rather than simply dual-band.

VI. Discussion of Vehicular Integration

A vehicular antenna must operate within severe packaging constraints. Roof modules, fascia-mounted sensors, pillars, and other body locations impose restrictions on available area and installation height. The reported 80 mm × 80 mm footprint is therefore relevant because it offers a compact starting point for integration. The single-layer planar structure also avoids the additional fabrication and alignment complexity associated with stacked multilayer architectures.

The shared-aperture concept can reduce the number of physical antenna modules needed for communication and sensing. In an integrated vehicle platform, this can simplify the RF front-end layout and provide a common mechanical reference for the two functions. However, practical integration introduces effects not evaluated in the supplied conference paper, including the presence of vehicle body metal, radome materials, mounting brackets, nearby electronics, cable routing, temperature, and manufacturing tolerances. These effects should be included in a subsequent validation stage rather than assumed to be negligible.

The proposed architecture is also scalable. The current configuration uses four radiating elements, but the same design philosophy could be extended toward larger arrays. Increasing the number of elements could provide additional degrees of freedom for beamforming and spatial processing. Such an extension would require a new optimization because larger arrays introduce additional coupling paths and a more complex feeding network. The current 2×2 design is therefore best viewed as a compact proof-of-concept architecture for the joint-function antenna concept.

Volume 10, Issue 9, pp. 32-40, September 2026. ISSN (Online): 2456-7361

VII. Comparison With Conventional Approaches

The conference manuscript contrasts the proposed architecture with conventional dual-band MIMO antennas that use stacked substrates or parasitic decoupling elements. Those approaches can provide strong electromagnetic performance, but they may increase thickness, fabrication complexity, or mechanical sensitivity. The present design instead uses a single-layer structure and incorporates the DGS into the ground plane.

A separate-antenna implementation has an obvious advantage in that each radio function can be optimized independently. Its disadvantages are the additional hardware footprint and the need to coordinate multiple physical antenna locations. A shared-aperture design reverses this trade-off: it improves packaging efficiency and functional integration, but the electromagnetic optimization becomes more coupled. The proposed antenna demonstrates that the latter problem can be managed through interleaved element placement, controlled feeds, tuning stubs, and DGS-based isolation.

TABLE 4: Advantage and challenges Comparision

Architecture	Primary advantage	Primary challenge	Relation to proposed design
Separate V2X + radar antennas	Independent optimization	Larger hardware footprint	Proposed design shares one aperture
Stacked dual-band MIMO	Strong frequency integration	Higher structural complexity	Proposed design uses single layer
Parasitic decoupling	Can improve isolation	Adds elements and tuning variables	Proposed design uses DGS
Proposed interleaved 2×2	Compact shared aperture; low ECC	Requires joint EM optimization	Validated in HFSS

This comparison is qualitative because the supplied conference paper does not provide a common numerical benchmark table for competing antennas. Accordingly, no unsupported comparative numerical claims are introduced.

VIII. Design Trade-Offs and Practical Limitations

The first trade-off is between compactness and coupling. Bringing the radiators into one module improves packaging efficiency but creates additional electromagnetic interaction. The DGS addresses one important coupling mechanism, yet the complete response remains dependent on element spacing, feed geometry, and ground currents. The second trade-off is between bandwidth and selectivity. The design must maintain distinct resonances at two widely separated frequencies while avoiding excessive interaction between them.

A third trade-off concerns radiation behavior. The V2X and radar functions do not require identical patterns. The communication band benefits from stable broadside coverage, whereas the radar band benefits from increased directivity. The reported patterns indicate that the proposed architecture naturally provides these different behaviors. A future vehicle-level implementation should nevertheless optimize the pattern for the exact mounting position because the vehicle body can transform a nominally broadside pattern.

The fourth limitation is the current reliance on full-wave simulation. The reported results are generated in HFSS and therefore demonstrate electromagnetic feasibility, but they do not constitute experimental validation. The source explicitly identifies experimental validation as future work. A rigorous journal follow-up should fabricate the antenna, measure S-parameters and far-field patterns, and compare the measured results against the simulated data under both free-space and representative vehicle-mounted conditions.

Finally, the present design is a 2×2 architecture. While it establishes low ECC and useful isolation, larger arrays would be needed for advanced spatial beamforming and higher-resolution radar sensing. Scaling should be performed systematically because additional elements increase the number of coupling paths and the complexity of the feed network.

IX. Implications for Joint Communication and Sensing

The proposed antenna is relevant to the broader idea of integrated sensing and communication because it provides a physical RF platform in which communication and sensing occupy the same mechanical aperture. The architecture does not claim waveform-level joint processing; rather, it addresses the antenna-level integration problem that precedes such processing. This distinction is important: an integrated RF aperture can reduce hardware duplication even when the communication and radar transceivers remain functionally distinct.

At the system level, the two bands can be treated as complementary resources. The 5.9 GHz channel offers a lower-frequency communication path with comparatively broad radiation, while the 24 GHz channel offers a higher-frequency and more directive sensing path. The MIMO arrangement provides spatial diversity for the communication function and a basis for future beamforming for the radar function. Consequently, the antenna can serve as a physical building block for a larger vehicle connectivity-and-sensing architecture.

The low ECC reported in the simulation is particularly important for this vision because spatial correlation can limit the practical benefit of multiple ports. The combination of ECC below 0.05 and isolation above 18 dB indicates that the four-port structure retains useful spatial independence in the simulated environment. Further system-level work should connect these antenna metrics to link-level throughput, radar detection performance, and robustness under realistic vehicle dynamics.

X. Future Work

Several extensions follow directly from the present results. First, the antenna should be fabricated and experimentally characterized. Second, beamforming networks can be integrated with the 24 GHz elements to evaluate electronic steering and directional sensing. Third, a larger MIMO configuration can be investigated to increase spatial degrees of freedom. Fourth, the architecture can be extended toward higher-frequency vehicular radar bands. Finally, vehicle-mounted simulations and measurements should be performed to quantify the influence of body structure and installation environment.

The optimization framework can also be expanded beyond electromagnetic objectives. A future design could simultaneously consider mechanical packaging, thermal constraints, manufacturing tolerances, RF efficiency, and link-level performance. Such a multidisciplinary workflow would move the design from a simulation-validated antenna toward a vehicle-ready module.

XI. Conclusion

This journal manuscript has expanded the supplied conference work on a dual-function 2×2 MIMO patch antenna for joint V2X communication and automotive radar. The proposed architecture integrates 5.9 GHz and 24 GHz radiators into a shared 80 mm × 80 mm planar aperture using interleaved rectangular patches, 50-Ω coaxial-fed wave ports, microstrip tuning stubs, and a DGS for isolation enhancement. The design addresses the central challenge of combining two widely separated operating frequencies while preserving MIMO diversity.

The reported HFSS results demonstrate −27 dB minimum S11 at 5.9 GHz and −22 dB at 24 GHz, isolation better than 18 dB, ECC below 0.05, and peak gains of approximately 7.5 dBi and 14.9 dBi, respectively. The radiation patterns remain stable at the communication band and become more directive at the radar band. These results collectively support the feasibility of the shared-aperture concept.

The main value of the design is the integration of several requirements within a compact and fabrication-friendly structure rather than optimization of a single antenna metric. The architecture provides a promising platform for connected-vehicle systems in which communication and sensing must coexist within constrained vehicle packaging. Experimental validation, vehicle-level characterization, beamforming, larger arrays, and extension to higher-frequency radar bands remain important directions for future work.

XII. Extended Electromagnetic Interpretation

The reported results can be interpreted as the outcome of a coordinated electromagnetic design rather than as independent optimizations of four isolated patches. In a multiport antenna, the resonant frequency of one element is affected by the current distribution established by the other elements, particularly when the radiators share the same ground plane. The interleaved arrangement therefore creates a coupled electromagnetic environment in which the feed geometry, patch dimensions, ground current, and DGS features must be considered together. The reported deep S11 minima at both operating frequencies indicate that the final geometry successfully restores the desired input impedance after these interactions are included in the full-wave model.

A. Relationship Between Resonance and Coupling

At 5.9 GHz, the electrical dimensions of the lower-band patches are relatively large compared with the 24 GHz elements. This difference allows the higher-frequency elements to be placed within the same overall board without requiring a second physical module. However, the common ground plane remains electrically active at both frequencies. The DGS therefore performs an important dual role: it changes the ground-current distribution while also limiting the propagation path through which neighboring ports can exchange energy. The reported isolation above 18 dB suggests that this approach is effective across both frequency regions.

B. Role of the Feed Network

The use of explicit microstrip feed lines and 50-Ω coaxial-fed wave ports makes the simulation closer to a realizable hardware configuration than an idealized lumped-port model. The source reports that microstrip tuning stubs were introduced to compensate for coupling-induced frequency shifts. This observation is important because the final resonant frequency of a MIMO element is not determined solely by the patch dimensions. Feed discontinuities, nearby radiators, and the ground-plane slots all contribute to the effective impedance seen by the port. The deeper resonance nulls reported after optimization therefore indicate successful coordination between the radiator and feed structure.

C. Current-Distribution Perspective

The gain enhancement at 24 GHz is attributed in the source to reduced surface-wave losses and improved current confinement. This interpretation is consistent with the purpose of the DGS: suppressing unwanted ground currents can redirect a greater fraction of the excited electromagnetic energy toward the intended radiator and free-space mode. At the lower frequency, the broader radiation behavior is maintained, which is appropriate for a communication function that does not require the same degree of spatial concentration as the radar channel. The two bands consequently exploit different electromagnetic characteristics of the same physical platform.

XIII. MIMO Metrics Beyond S-Parameters

A central strength of the proposed architecture is the use of multiple MIMO metrics rather than relying only on the reflection coefficient. S11 verifies that a port is matched, but it does not indicate whether the antenna elements behave independently. S21 and related coupling terms provide that additional information, while ECC gives a direct diversity-oriented interpretation. The reported combination of isolation better than 18 dB and ECC below 0.05 indicates that the antenna retains low inter-port interaction and low spatial correlation in the simulated bands.

A. Significance of Low ECC

For a communication MIMO system, low correlation is valuable because the individual ports can provide more distinct spatial channels. In the proposed antenna, the low ECC is achieved through the combined effect of physical arrangement and coupling suppression. The result is particularly relevant to the shared-aperture concept: if the radar elements or communication elements strongly correlated with one another, adding multiple ports would provide limited practical diversity benefit. The reported ECC below 0.05 demonstrates that the four-port architecture is not merely a collection of resonators but a functioning MIMO structure.

B. Isolation Versus Physical Footprint

Isolation enhancement is often accompanied by additional spacing, parasitic elements, neutralization structures, or multilayer configurations. The proposed design takes a different route by modifying the ground plane. This is attractive for vehicle packaging because the overall footprint remains 80 mm × 80 mm. The approach also avoids introducing a separate decoupling network that would need to be tuned for two widely separated bands. The trade-off is that DGS geometry becomes another fabrication-sensitive feature and should therefore be evaluated carefully in future prototype work.

XIV. Sensitivity to Practical Vehicle Conditions

Although the supplied results are based on a free-space HFSS model, the intended application is vehicular. A practical installation can place the antenna near conductive body panels, painted surfaces, radomes, brackets, and other RF structures. These nearby materials can shift resonant frequencies and modify the radiation pattern. The lower 5.9 GHz band is particularly sensitive to the effective electrical environment because its wavelength is substantially longer, while the 24 GHz band can be strongly affected by relatively small mechanical features because they represent a larger electrical size at mmWave frequencies.

A. Mounting and Packaging

The planar architecture provides flexibility for mounting, but the final installation location should be selected together with the RF simulation model. The reported 80 mm × 80 mm board size is a useful module-level constraint, yet the usable electromagnetic aperture is determined by the surrounding vehicle geometry. A future study should therefore compare free-space performance with representative roof, fascia, or other candidate mounting conditions. Such analysis would identify frequency shifts, pattern distortion, gain changes, and any degradation in isolation caused by the vehicle structure.

B. Environmental and Manufacturing Considerations

Temperature, material-property variation, fabrication tolerances, connector placement, and DGS etching accuracy can all influence a compact dual-band MIMO antenna. The supplied conference paper does not report a tolerance analysis or measured prototype, so these effects remain open questions. A journal validation campaign should vary the critical geometric parameters and substrate properties around their nominal values and identify which variables dominate the two resonances and the isolation response. The resulting sensitivity information would help prioritize manufacturing controls and mechanical tolerances.

XV. Recommended Experimental Validation Framework

The next stage of the work should be organized around a direct simulation-to-measurement comparison. The fabricated prototype should first be characterized with a calibrated vector network analyzer to obtain the four-port S-parameter matrix. The measured S11 and isolation curves can then be compared with the HFSS results at 5.9 GHz and 24 GHz. Because the antenna is intended for two distinct functions, the measurement plan should preserve the distinction between the broadside communication behavior at the lower band and the more directive radar behavior at the higher band.

A. Network-Parameter Measurements

A four-port measurement provides the most direct validation of the MIMO model. Each port should be characterized while the remaining ports are terminated according to the measurement configuration. The measured resonance frequencies, return loss, and coupling terms should be compared against the simulated curves. Differences can be attributed systematically to connector transitions, substrate-property variation, fabrication tolerances, or mounting effects rather than treated as unexplained discrepancies.

B. Far-Field Measurements

The simulated radiation patterns in Fig. 4 provide a reference for anechoic-chamber characterization. Measurements should determine whether the 5.9 GHz pattern remains broadside and whether the 24 GHz pattern retains the reported increased directivity. Peak gain should also be measured independently at both bands. Because the source reports gains of 7.5 dBi and 14.9 dBi, the experimental campaign can use these values as baseline targets rather than as assumed measured performance.

C. Vehicle-Level Validation

After free-space validation, the antenna should be evaluated in its intended vehicle location. This step is important because a shared communication-and-radar aperture may experience different installation constraints for the two functions. A vehicle-mounted measurement can reveal pattern blockage, changes in polarization behavior, resonant shifts, and coupling to nearby electronics. Such testing would convert the present electromagnetic proof of concept into evidence of practical integration feasibility.

XVI. Scalability Toward Larger MIMO Arrays

The 2×2 configuration establishes the basic dual-band architecture but also provides a natural starting point for larger arrays. Scaling to 4×4 or other configurations could increase spatial degrees of freedom for communication beamforming and radar processing. The main challenge is that the number of coupling paths increases rapidly as more elements are introduced. Consequently, the DGS arrangement and feed network would need to be redesigned rather than simply replicated without further optimization.

International Journal of Scientific Engineering and Science
Volume 10, Issue 9, pp. 32-40, September 2026. ISSN (Online): 2456-7361

A. Beamforming Opportunity

The more directive 24 GHz response is particularly compatible with future beamforming. If individual element phases and amplitudes are controlled, the array can potentially form directional beams for radar sensing or high-data-rate links. The current conference paper does not include a beamforming network or steering results, so such functionality should be considered a future extension. The existing low-correlation and high-isolation results nevertheless provide a useful electromagnetic foundation for that extension.

B. Higher-Frequency Extension

The same integration philosophy can also be considered for higher-frequency vehicular radar bands. At higher frequencies, the physical dimensions become smaller, which can enable additional elements within a constrained aperture. At the same time, conductor loss, dielectric loss, fabrication accuracy, and mechanical tolerances become increasingly important. Any higher-frequency extension would therefore require a new optimization and validation process rather than a direct geometric scaling of the present design.

XVII. Broader Engineering Significance

The principal contribution is architectural: V2X communication and radar share a compact planar electromagnetic platform. The results show that this integration can be achieved without a multilayer structure or complex external decoupling network. Related work has separately addressed automotive radar arrays [8], [17]–[20] and MIMO isolation using DGS or parasitic decoupling [21]–[25], whereas the present architecture combines the two functions in one dual-band planar module.

A. Relevance to Intelligent Transportation Systems

Future transportation platforms are expected to combine connectivity, perception, localization, and increasingly automated decision-making. An antenna that supports communication and sensing within one module can contribute to this convergence at the physical layer. The present work focuses specifically on the antenna, so it does not claim end-to-end joint radar-communication processing. Its value is instead the creation of a compact RF aperture that can serve as a foundation for subsequent transceiver and signal-processing integration.

B. Research Reproducibility and Scope

The supplied conference paper provides the essential architecture, HFSS methodology, operating frequencies, overall footprint, and principal performance results. It does not provide every individual geometric dimension, mesh image, fabrication drawing, or measured dataset. The journal extension therefore preserves those boundaries. A complete reproducibility package would ideally include the HFSS project, exact patch and DGS dimensions, material stack-up, port definitions, mesh statistics, and exported S-parameter data. Providing those artifacts in future work would allow independent researchers to reproduce the reported curves and systematically compare alternative isolation techniques.

Acknowledgment

I would like to acknowledge the support provided by simulation tools such as Ansys HFSS, grammarly to check spellings. Special thanks are extended to the automotive communication labs and academic reviewers for their valuable insights during the development phase.

References

[1] H. Tataria , "6G Wireless Systems: Vision, Requirements, Challenges, Insights, and Opportunities," Proc. IEEE, vol. 109, no. 7, pp. 1166–1199, Jul. 2021.
[2] H. Yejun., "Leaky-Wave Antennas for 5G/B5G Mobile Communication Systems: A Survey," ZTE Commun., vol. 18, no. 3, pp. 9–16, 2020.
[3] S. Kim , "Design Considerations for mmWave Phased Arrays," IEEE Trans. Antennas Propag., vol. 67, no. 5, pp. 3198–3207, May 2019.
[4] C. Caloz and T. Itoh, Electromagnetic Metamaterials: Transmission Line Theory and Microwave Applications. Wiley, 2005.
[5] M. Giordani, "Toward 6G Networks: Use Cases and Technologies," IEEE Commun. Mag., vol. 58, no. 3, pp. 55–61, Mar. 2020.
[6] D. Liu , "Advanced Antenna Systems for 5G and Beyond," IEEE J. Microwaves, vol. 1, no. 1, pp. 232–242, Jan. 2021.
[7] D. R. Jackson and A. A. Oliner, "Leaky-Wave Antennas," in Modern Antenna Handbook, J. L. Volakis, Ed. Wiley, 2008.
[8] S. Lim, "Metamaterial-Based Electrically Small Leaky-Wave Antennas for Beam Scanning Applications," IEEE Trans. Antennas Propag., vol. 53, no. 1, pp. 161–168, Jan. 2005.
[9] A. Ahmed , "A Survey on Dual-Function Radar Communication Systems," IEEE Commun. Surveys Tuts., vol. 24, no. 1, pp. 517–547, 1st Quart. 2022.
[10] H. Zhu, M. Ansari, and Y. Jay Guo, "Wideband beam-forming networks utilizing planar hybrid couplers and phase shifters," IEEE Trans. Antennas Propag., vol. 70, no. 9, pp. 7592–7602, Sep. 2022.
[11] X.-X. Yang, H. Qiu, T. Lou, Z. Yi, Q.-D. Cao, and S. Gao, "Circularly polarized millimeter wave frequency beam scanning antenna based on aperture-coupled magneto-electric dipole," IEEE Trans. Antennas Propag., vol. 70, no. 9, pp. 7603–7611, Sep. 2022.
[12] X. Li, J. Wang, G. Goussetis, and L. Wang, "Circularly polarized high gain leaky-wave antenna for CubeSat communication," IEEE
[13] H. Zhang et al., "Reconfigurable reflectarray antenna based on hyperuniform disordered distribution," IEEE Trans. Antennas Propag., vol. 70, no. 9, pp. 7513–7523, Sep. 2022.
[14] F. A. Dicandia and S. Genovesi, "Wide-scan and energy-saving phased arrays by exploiting penrose tiling subarrays," IEEE Trans. Antennas Propag., vol. 70, no. 9, pp. 7524–7537, Sep. 2022.
[15] Y. Zeng, X. Ding, Y. Wang, W. Shao, and B.-Z. Wang, "A squarerate arrangement method for large-spacing planar phased array grating lobes homogenization," IEEE Trans. Antennas Propag., vol. 70, no. 9, pp. 7538–7545, Sep. 2022.
[16] T. S. Rappaport, S. Sun, R. Mayzus, H. Zhao, Y. Azar, K. Wang, G. N. Wong, J. K. Schulz, M. Samimi, and F. Gutierrez, "Millimeter Wave Mobile Communications for 5G Cellular: It Will Work!," IEEE Access, vol. 1, pp. 335–349, 2013, doi: 10.1109/ACCESS.2013.2260813.
[17] J. Choi, V. Va, N. González-Prelcic, R. Daniels, C. R. Bhat, and R. W. Heath, Jr., "Millimeter-Wave Vehicular Communication to Support Massive Automotive Sensing," IEEE Commun. Mag., vol. 54, no. 12, pp. 160–167, Dec. 2016, doi: 10.1109/MCOM.2016.1600071.
[18] S. M. Patole, M. Torlak, D. Wang, and M. Ali, "Automotive Radars: A Review of Signal Processing Techniques," IEEE Signal Process. Mag., vol. 34, no. 2, pp. 22–35, Mar. 2017, doi: 10.1109/MSP.2016.2628914.
[19] M. S. Pervez and A. Kaur, "Design of a Compact Size Bridge Connected Multiband MIMO Antenna for Wireless Applications," conference publication supplied by the authors.
[20] S. Sun and T. S. Rappaport, "MIMO for Millimeter-Wave Wireless Communications: Beamforming, Spatial Multiplexing, or Both?," IEEE Commun. Mag., vol. 52, no. 12, pp. 110–121, Dec. 2014.
[21] "Study of a 5.8 GHz Frequency Band Patch Antenna Integrated Into a Vehicle for Automotive DSRC Applications," in Proc. IEEE Vehicular Technology Conference, IEEE, 2007, document record available in IEEE Xplore.

[22] P. Kumari, N. J. Myers, and R. W. Heath, Jr., "Adaptive and Fast Combined Waveform-Beamforming Design for mmWave Automotive Joint Communication-Radar," IEEE J. Sel. Topics Signal Process., vol. 15, no. 4, pp. 996–1012, Aug. 2021, doi: 10.1109/JSTSP.2021.3071592.
[23] C.-A. Yu, K.-S. Chin, and R. Lu, "24-GHz Wide-Beam Patch Antenna Array Laterally Loaded With Parasitic Strips," in Proc. 2019 Cross Strait Quad-Regional Radio Science and Wireless Technology Conference (CSQRWC), 2019, doi: 10.1109/CSQRWC.2019.8799203.
[24] J. A. Zhang, X. Huang, Y. J. Guo, J. Yuan, and R. W. Heath, Jr., "Multibeam for Joint Communication and Radar Sensing Using Steerable Analog Antenna Arrays," IEEE Trans. Veh. Technol., vol. 68, no. 1, pp. 671–685, Jan. 2019.
[25] A. Alkhateeb, G. Leus, and R. W. Heath, Jr., "Limited Feedback Hybrid Precoding for Multi-User Millimeter Wave Systems," IEEE Trans. Wireless Commun., vol. 14, no. 11, pp. 6481–6494, Nov. 2015.
[26] M. Giordani, M. Polese, A. Roy, D. Castor, and M. Zorzi, "Toward 6G Networks: Use Cases and Technologies," IEEE Commun. Mag., vol. 58, no. 3, pp. 55–61, Mar. 2020.
[27] K. V. Mishra, M. R. Bhavani Shankar, V. Koivunen, B. Ottersten, and S. A. Vorobyov, "Toward Millimeter-Wave Joint Radar Communications: A Signal Processing Perspective," IEEE Signal Process. Mag., vol. 36, no. 5, pp. 100–114, Sep. 2019, doi: 10.1109/MSP.2019.2913173.
[28] X. Wang, W. Zhai, X. Zhang, X. Wang, and M. G. Amin, "Enhanced Automotive Sensing Assisted by Joint Communication and Cognitive Sparse MIMO Radar," IEEE Trans. Aerosp. Electron. Syst., vol. 59, no. 5, pp. 4782–4799, Oct. 2023.
[29] D. Srivastava and R. K. Gangwar, "Wideband Conformal MIMO 5G Antenna System for Millimeter-Wave Vehicle-to-Everything (V2X) Communications," in Proc. IEEE Asia-Pacific Conf. Applied Electromagnetics (APACE), 2024, doi: 10.1109/APACE62360.2024.10877398.
[30] J. A. Zhang et al., "Transmit Waveform Design for Integrated Wideband MIMO Radar and Bi-Directional Communications," IEEE Trans. Veh. Technol., vol. 73, no. 9, pp. 13482–13497, Sep. 2024.
[31] "A 24 GHz MIMO PMCW Automotive Radar with Doppler Compensation," IEEE conference publication, IEEE Xplore document 9499640.
[32] T.-H. Le, M. Kaiser, I. Ndip, M. Schiffer, and M. Schneider-Ramelow, "3D Mold Embedded PCB-Based MIMO Antenna Arrays for 79 GHz Automotive RADAR," in Proc. European Radar Conf. (EuRAD), 2023, doi: 10.23919/EuRAD58043.2023.10289146.
[33] "Procedure to Design a Series-fed Microstrip Patch Antenna Array for 77 GHz Automotive Radar," IEEE conference publication, IEEE Xplore document 8799356.
[34] "8×8 Millimeter-Wave Series-Fed Patch Antenna Array for Anti-Collision Automotive Radar," IEEE conference publication, IEEE Xplore document 9886629.
[35] "Automotive MIMO Radar Angle Estimation in the Presence of Multipath," IEEE conference publication, IEEE Xplore document 8249152.
[36] MOHAMMAD SHAHED PERVEZ and AMANPREET KAUR. A dual-mode leaky-wave antenna for scanning beam applications in 6g communication and automotive radar systems. World Journal of Advanced Engineering Technology and Sciences, 2025, 15(02), 2219-2226. Article DOI: https://doi.org/10.30574/wjaets.2025.15.2.0785.